AD NUMBER

AD921318

LIMITATION CHANGES

TO:

Approved for public release; distribution is unlimited.

FROM:

Distribution authorized to U.S. Gov't. agencies only; Administrative/Operational Use; APR 1974. Other requests shall be referred to Air Force Armament Lab., Eglin AFB, FL.

AUTHORITY

USADTC ltr 30 May 1979

TECHNICAL REPORT AFATL-TR-74-84

FUNDAMENTAL PARAMETERS AFFECTING PLUME INFRARED RADIATION

AEROSPACE TARGETS BRANCH
AIR-TO-AIR MISSILES AND TARGETS DIVISION

APRIL 1974

FINAL REPORT: July 1973 to February 1974

AIR FORCE ARMAMENT LABORATORY
AIR FORCE SYSTEMS COMMAND • UNITED STATES AIR FORCE
EGLIN AIR FORCE BASE, FLORIDA

UNCLASSIFIED
SECURITY CLASSIFICATION OF THIS PAGE (When Data Entered)

REPORT DOCUMENTATION PAGE		READ INSTRUCTIONS BEFORE COMPLETING FORM
1. REPORT NUMBER AFATL-TR-74-84	2. GOVT ACCESSION NO.	3. RECIPIENT'S CATALOG NUMBER
4. TITLE (and Subtitle) FUNDAMENTAL PARAMETERS AFFECTING PLUME INFRARED RADIATION		5. TYPE OF REPORT & PERIOD COVERED Final Report July 1973 - February 1974 6. PERFORMING ORG. REPORT NUMBER
7. AUTHOR(s) Dr. Davut B. Ebeoglu		8. CONTRACT OR GRANT NUMBER(s)
9. PERFORMING ORGANIZATION NAME AND ADDRESS Air-to-Air Missiles and Targets Division (DLQT) Air Force Armament Laboratory Eglin Air Force Base, Florida 32542		10. PROGRAM ELEMENT, PROJECT, TASK AREA & WORK UNIT NUMBERS P. E. 62602F Proj 19210301
11. CONTROLLING OFFICE NAME AND ADDRESS Air Force Armament Laboratory Air Force Systems Command Eglin Air Force Base, Florida 32542		12. REPORT DATE April 1974 13. NUMBER OF PAGES 32
14. MONITORING AGENCY NAME & ADDRESS(if different from Controlling Office)		15. SECURITY CLASS. (of this report) Unclassified 15a. DECLASSIFICATION/DOWNGRADING SCHEDULE

16. DISTRIBUTION STATEMENT (of this Report)
Distribution limited to U. S. Government agencies only; this report documents test and evaluation; distribution limitation applied April 1974. Other requests for this document must be referred to the Air Force Armament Laboratory (DLQT), Eglin Air Force Base, Florida 32542.

17. DISTRIBUTION STATEMENT (of the abstract entered in Block 20, if different from Report)

18. SUPPLEMENTARY NOTES
Available in DDC

19. KEY WORDS (Continue on reverse side if necessary and identify by block number)
Infrared Signature
Infrared Radiant Intensity
Oxidizer to Fuel Mixture Ratio
Choked Flow
Exhaust Plume
Infrared Simulation Techniques

20. ABSTRACT (Continue on reverse side if necessary and identify by block number)
The development of realistic aerial target systems for air-to-air missiles testing requires the capability to simulate the infrared signature of turbojet engine exhausts within the limited payload of a subscale airframe. Investigations are being performed to identify and understand the parameters that are most effective in maximizing the infrared radiant intensity from the plume of small engines. This report describes the results of experiments performed under static ambient conditions simulating altitudes up to 60,000 feet. The relationship between the infrared radiation emitted in the 3 to 5 micron band and the gas dynamics parameters has
(continued)

DD FORM 1 JAN 73 1473 EDITION OF 1 NOV 65 IS OBSOLETE

UNCLASSIFIED
SECURITY CLASSIFICATION OF THIS PAGE (When Data Entered)

Item 20. Continued
been studied. Two major parameters, oxidizer to fuel mixture ratio and choked flow, have been identified which will cause order of magnitude variations in plume infrared radiant intensity. Total mass flow and chamber pressure have been found to be secondary parameters which cause linear variations in radiant intensity in this band. Exit gas velocity and thrust were found to have very little effect on the infrared figure of merit, J. Radiant intensity was normalized to mass flow rate in this investigation and designated as $\bar{J}$ (watts/steradian output divided by total mass flow rate input) so as to obtain a direct indication of target drone payload requirements for a given source as well as predicting the duration of the simulation.

PREFACE

This technical report describes the results of work performed under Project 19210301, Infrared Simulation Techniques, in support of Program Element 62602F. The entire effort was conducted in-house in the Aerospace Targets Branch (DLQT) of the Air Force Armament Laboratory, Eglin Air Force Base, Florida. The work described covers the period 1 July 1973 through 1 February 1974. The experimental measurements described were performed by Lt. Charles W. Martin, Mr. Dale E. Fink, and Dr. Kenneth E. Harwell, consultant (Auburn University) as well as the author, Dr. Davut B. Ebeoglu.

This report has been reviewed and is approved.

JOHN W. JOHNSON
Acting Chief, Air-to-Air Missiles
and Targets Division

(The reverse of this page is blank)

TABLE OF CONTENTS

(The reverse of this page is blank)

SECTION I

INTRODUCTION

Subscale aerial targets with limited payloads are required to simulate full-scale threat turbojet engine exhaust plumes over a wide range of flight envelopes. These requirements result in a need for a thorough understanding and optimization of the fundamental parameters which affect the infrared radiation of sources that can be carried on aerial targets. These targets must simulate threat aircraft exhaust plumes at operational altitudes which range from sea level to not more than 100,000 feet and flight speeds which go from near static to Mach 4.

This report describes the results of an investigation at static altitudes to determine the relationship between plume infrared signatures in the 4 to 5 micron band and the gas dynamics operating conditions of a basic infrared simulation source. The objective of this parametric analysis has been to determine how radiation from an exhaust plume can be controlled. The most effective conditions for optimizing infrared radiant intensity have been determined.

The preliminary data obtained with a subscale rocket engine was reported earlier as were the conclusions reached on the data available at that time (Reference 1 and 2). Numerous experiments performed since then have yielded the remaining major combustion parameters which effect plume radiant intensity. At the same time the previous data have been studied further and earlier interpretations have been extended to their logical final conclusions.

The data described in this report were mostly obtained with the same subscale kerosene/oxygen rocket motor. The operating conditions encompassed total mass flows ranging from 3 to 10 grams/second, chamber pressures from 2 to 200 psi, and exit gas velocities from 500 to 2600 meters/second. The engine, which is shown in a cutaway drawing in Figure 1, has been described previously in additional detail (Reference 3). The altitude chamber shown in Figure 2 was used to vary the ambient altitude to 60,000 feet.

References:

1. Dr. D.B. Ebeoglu: A Preliminary Investigation of Rocket Engine Plume for Turbojet Simulation. Proceedings JANNAF 7th Plume Technology Meeting, pp. 569-576, CPIA Publication 234, June 1973.
2. Dr. D.B. Ebeoglu: Infrared Simulation of Turbojet Radiation. Proceedings 11th IRIS Symposium on Infrared Countermeasures, pp. 139-149, February 1974.
3. J.F. Long, Dr. D.B. Ebeoglu, Dr. K.E. Harwell: Infrared Plumes Simulation Test Facility Handbook. AFATL-TR-74-15, Eglin AFB, Florida, January 1974.

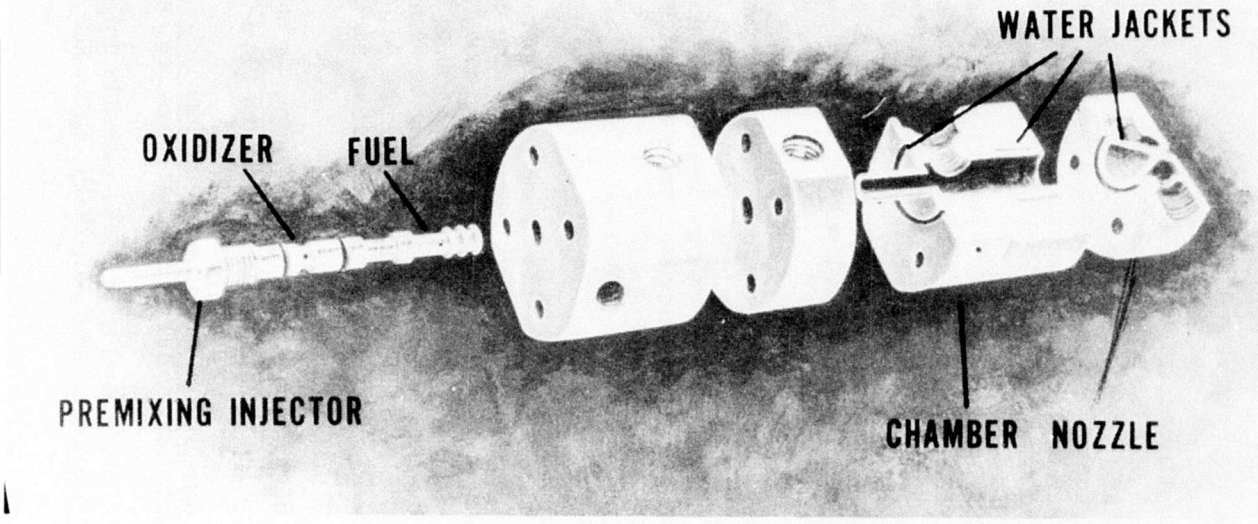

Figure 1. Subscale Kerosene/Oxygen Rocket Engine.

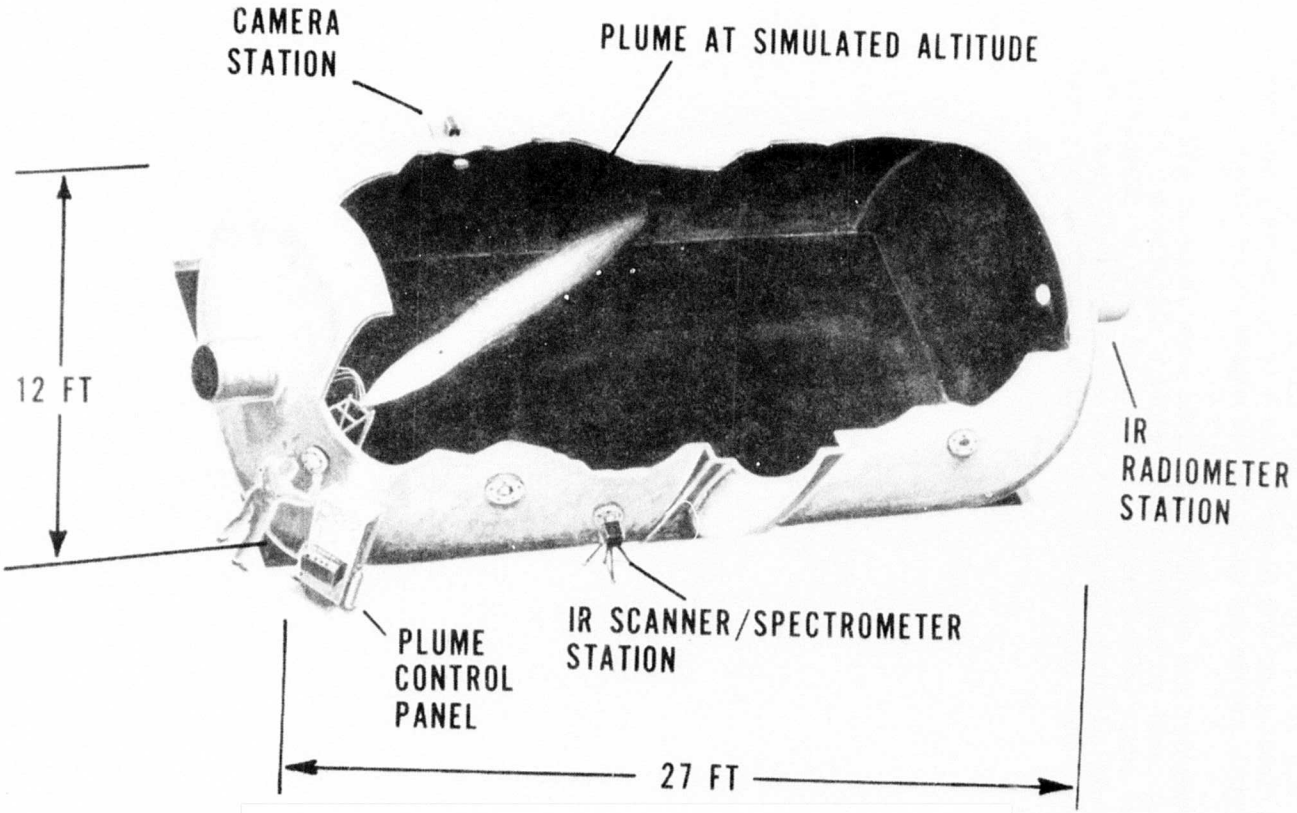

Figure 2. Altitude Simulation Test Facility.

Infrared radiant intensity measurements were obtained in the 4 to 5 micron band at an aspect angle of 30 degrees from the tail of the plume. The infrared spatial distribution of the plume in the 4 to 5.5 micron band was obtained with a thermal scanner by using the 90 degree angle window.

Combustion parameters and ambient conditions were isolated and studied individually in order to determine the relative significance of each. Variables that cause small variations in output could thus be identified and evaluated as could nonlinear parameters and boundary conditions. The approach taken allowed each parameter to be evaluated over its full range of realistic values.

SECTION III

STATIC ALTITUDE EFFECT

The shape of a rocket exhaust plume changes significantly with altitude. At sea level a supersonic exhaust plume has a characteristic double triangle shape (Shown in (a) of Figure 3) which consists of a core region which expands rapidly and which covers nearly all of the total length of the plume. As the altitude increases the expansion becomes more gradual and the length of the plume increases. The plume becomes narrower at the base while its length changes by a factor of 6 from sea level to 67,000 feet. The maximum width of the plume does not change appreciably with altitude; it only moves further downstream.

A number of shock diamonds are produced above a certain altitude depending on the exit gas velocity. Since exit gas velocity is dependent on chamber pressure and mass flow, the shock structure appears at different altitudes for different engine operating conditions. This shock region is followed by a fairly long afterburning section. A typical plume with such shock structure is shown in (b) of Figure 3.

Figure 4 illustrates the effect of altitude on plume length for a sonic and subsonic nozzle. This relationship generally holds for all types of plumes of interest. Plumes will differ in shape due to variations in expansion ratio and mixture ratio; however, the plume length is generally affected by altitude in the nonlinear manner shown in Figure 4. The variation in length can be empirically shown to be inversely proportional to the square root of the ambient atmospheric pressure.

Figure 5 shows the infrared image of a plume in the 4 to 5.5 micron infrared band. The two representations were created by digital data reduction routines from a matrix of 56 X 94 radiant intensity points obtained by a thermal scanner. In Figure 5(a) the width of shading is used to indicate the level of radiant intensity, much in the same manner as in radioisotope scanner displays. Sixteen levels are used to cover the dynamic range of the data. In Figure 5(b) the radiant intensity of the same plume is shown as the third dimension off the x-y base.

There are islands in the plume (for instance, at various shock regions) that emit more than the surrounding volume of gas. However, the total radiant intensity of a plume appears to be a function of the total volume (including the afterburning regions) rather than the sum of these islands of high radiation. The detailed distribution of infrared radiation over the plume volume and surface

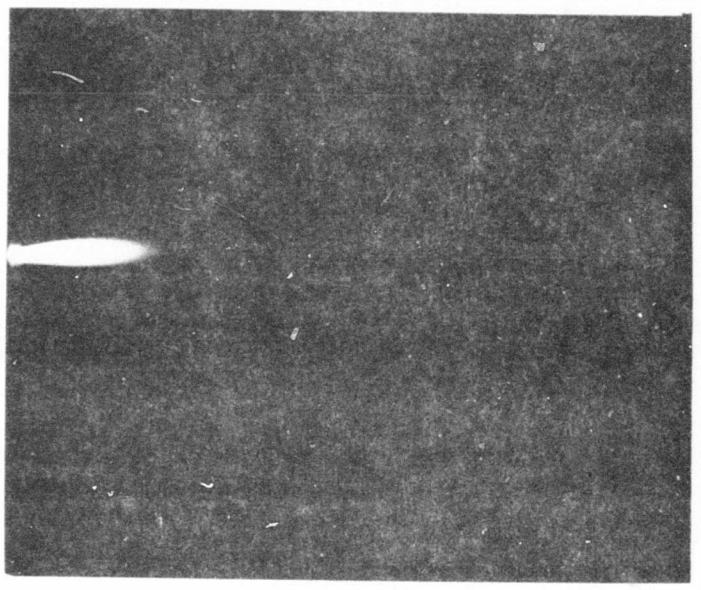

(a) Sea Level.

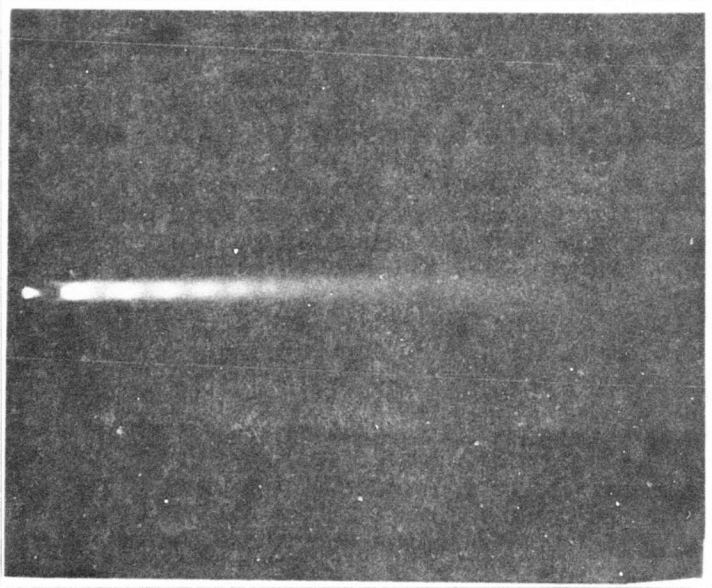

(b) 40,000 Feet.

Figure 3. Exhaust Plume Geometry at Sea Level and at 40,000 Feet.

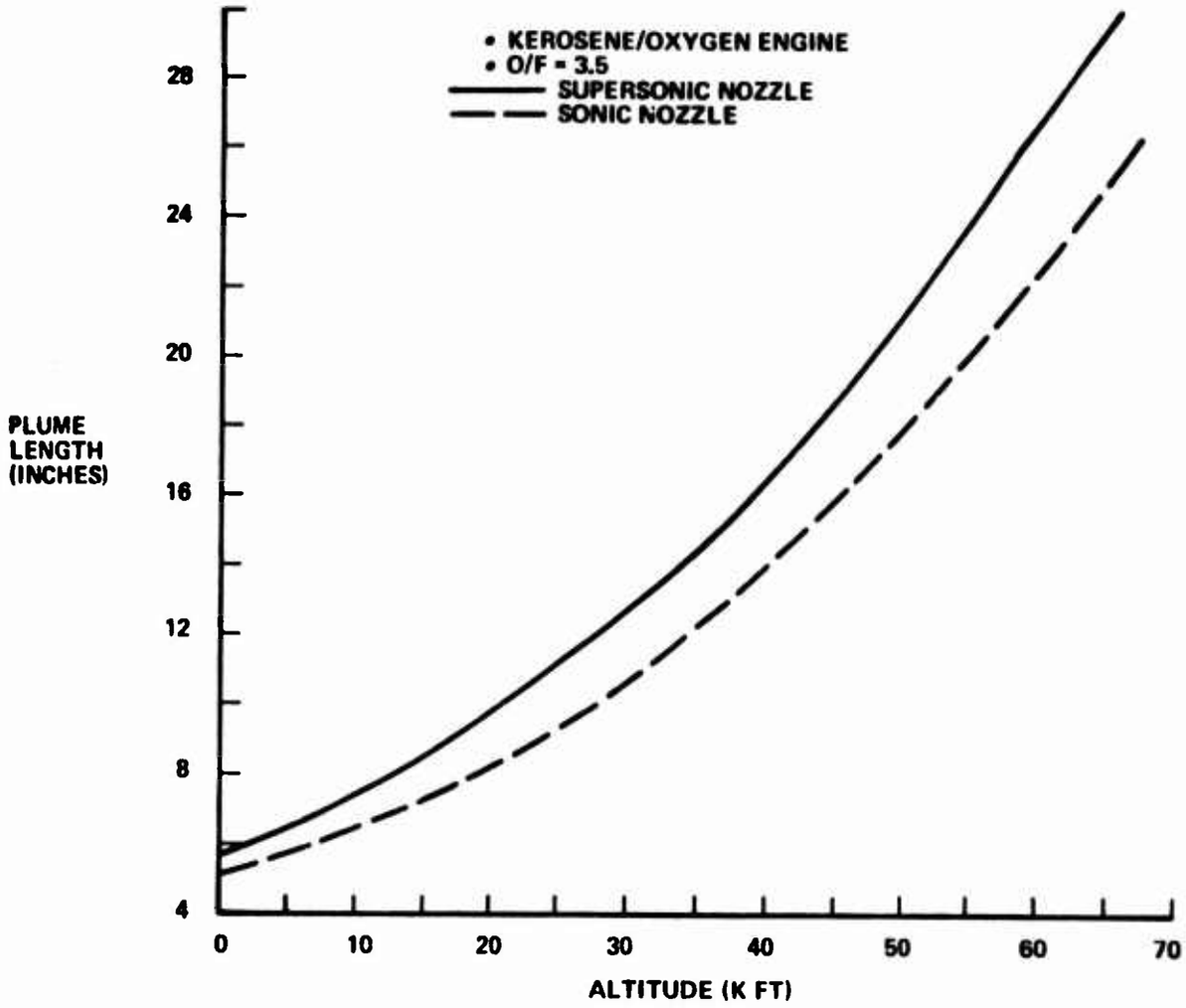

Figure 4. Effect of Altitude on Plume Length

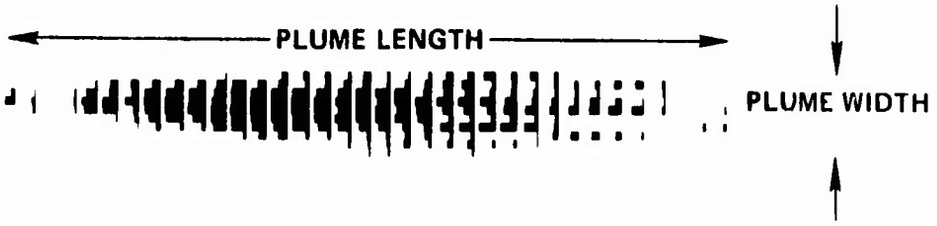

(a)

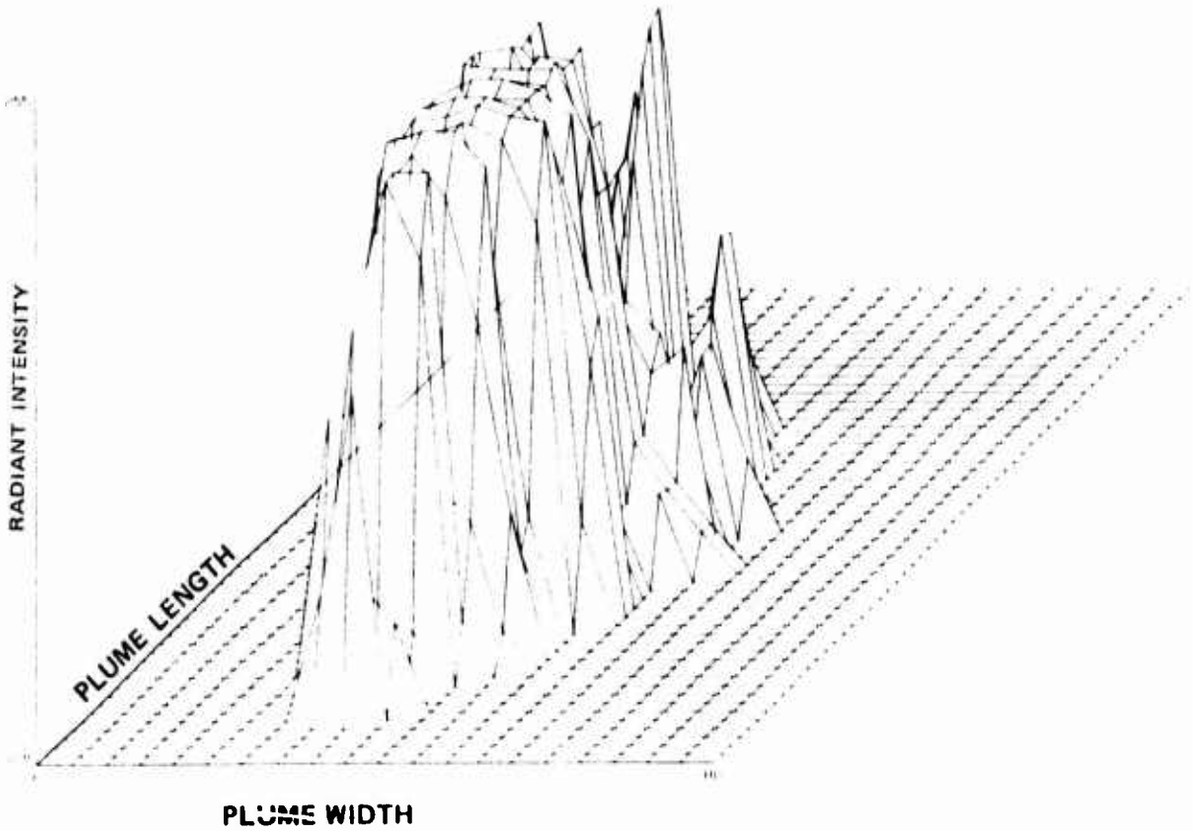

(b)

Figure 5. Plume Infrared Distribution in the 4 to 5.5 Micron Band

is being studied at this time with the thermal scanner as a function of mass flow, mixture ratio as well as altitude and will be described in a future report.

The effect of altitude on the infrared signature thus closely parallels the effect of altitude on the shape of the plume. Figure 4 illustrates the effect of altitude on the infrared figure of merit as well as on plume length. Although the data shown were taken at an aspect angle of 30 degrees, the relationship holds for all aspect angles.

SECTION III

OXYGEN/FUEL RATIO EFFECT

The major parameter which controls the infrared radiation from a plume is the O/F ratio (Reference 1 and 2). Figure 6 shows the preliminary relationship between radiant intensity and mixture ratio at a static altitude of 60,000 feet as presented earlier. The radiant intensity is normalized to a performance figure of merit. The normalized unit, designated $\bar{J}$ (watts/steradian/gram/second) is used to relate radiant intensity (watts/steradian) to the combined mass flow of oxidizer and fuel into the engine (grams/second). The engine infrared performance can thus be immediately evaluated in terms of the payload required and the burn duration in a subscale target drone.

Detailed observations and analyses have now been performed which result in the conclusion that the definitive relationship between $\bar{J}$ and O/F ratio is as shown in Figure 7. Two earlier observations are significant: (1) a maximum $\bar{J}$ is produced at an O/F ratio well below the stoichiometric ratio of 3.4 for a kerosene/oxygen mixture, (2) the value of O/F ratio at which the maximum $\bar{J}$ occurs increases with altitude.

Subsequently, the following have been noted: (1) The plume produced below the optimum O/F ratio has a yellow-red color; it contains particulate carbon as well as unburned fuel mixed in with the gaseous plume (if the engine is operated at these low O/F ratios for several minutes, the unburned atomized fuel collected in the altitude chamber ignites in a giant fireball). Increasing the fuel flow to operate at even lower O/F ratios, produces a sootier exhaust and decreases the plume size. These observations leave little doubt that the exhaust plume is fuel-rich at operating conditions below the optimum O/F ratio. (2) The plume turns greenish and then blue-white as the O/F ratio is increased above the optimum. The color remains blue-white as the oxygen is increased while the plume length decreases These lead to the conclusions that the exhaust plume becomes oxygen-rich once past the optimum O/F ratio.

The variation in the plume geometry and color as a function of O/F ratio is illustrated in Figure 8. These observations, coupled to the earlier data, lead to the conclusion that the maximum plume volume (and thus the maximum infrared radiant intensity) occurs when stoichiometric conditions prevail within the boundaries of the plume rather than in the combustion chamber. This optimum condition then is a function of the unburned fuel in the exhaust (which must exist since combustion within the engine is occurring below the O/F ratio of 3.4) and the oxygen in the ambient.

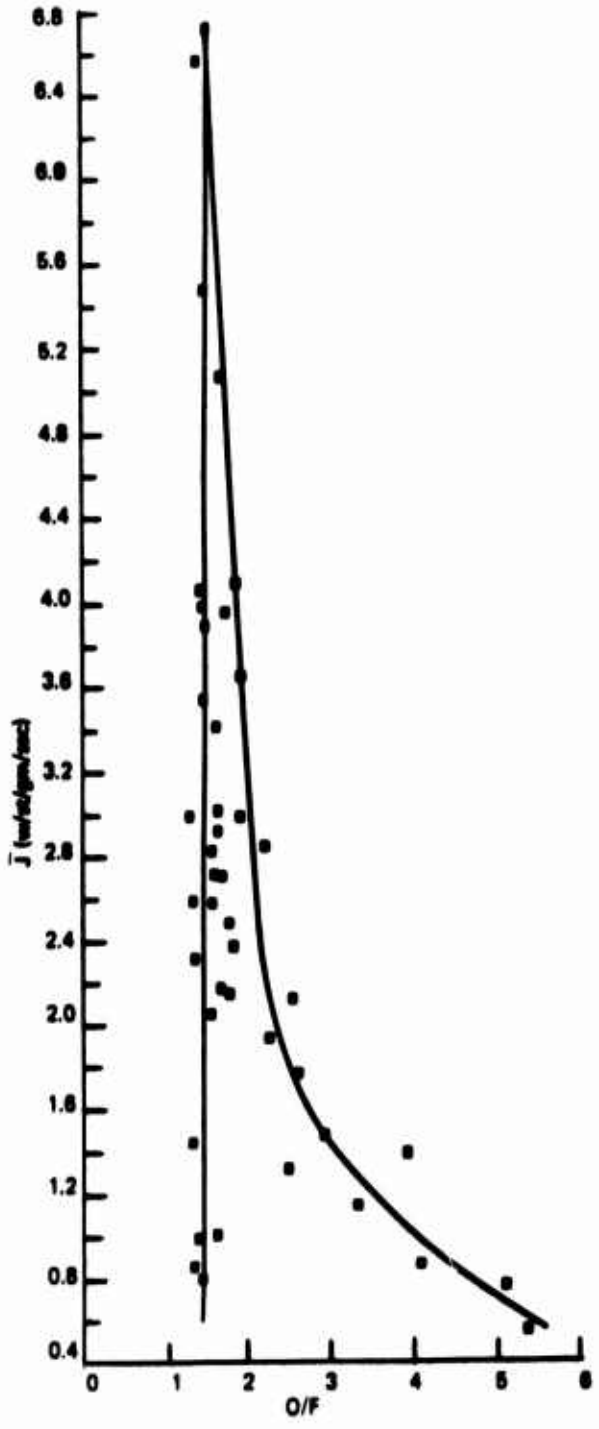

Figure 6. Preliminary Relationship between $\bar{J}$ and O/F

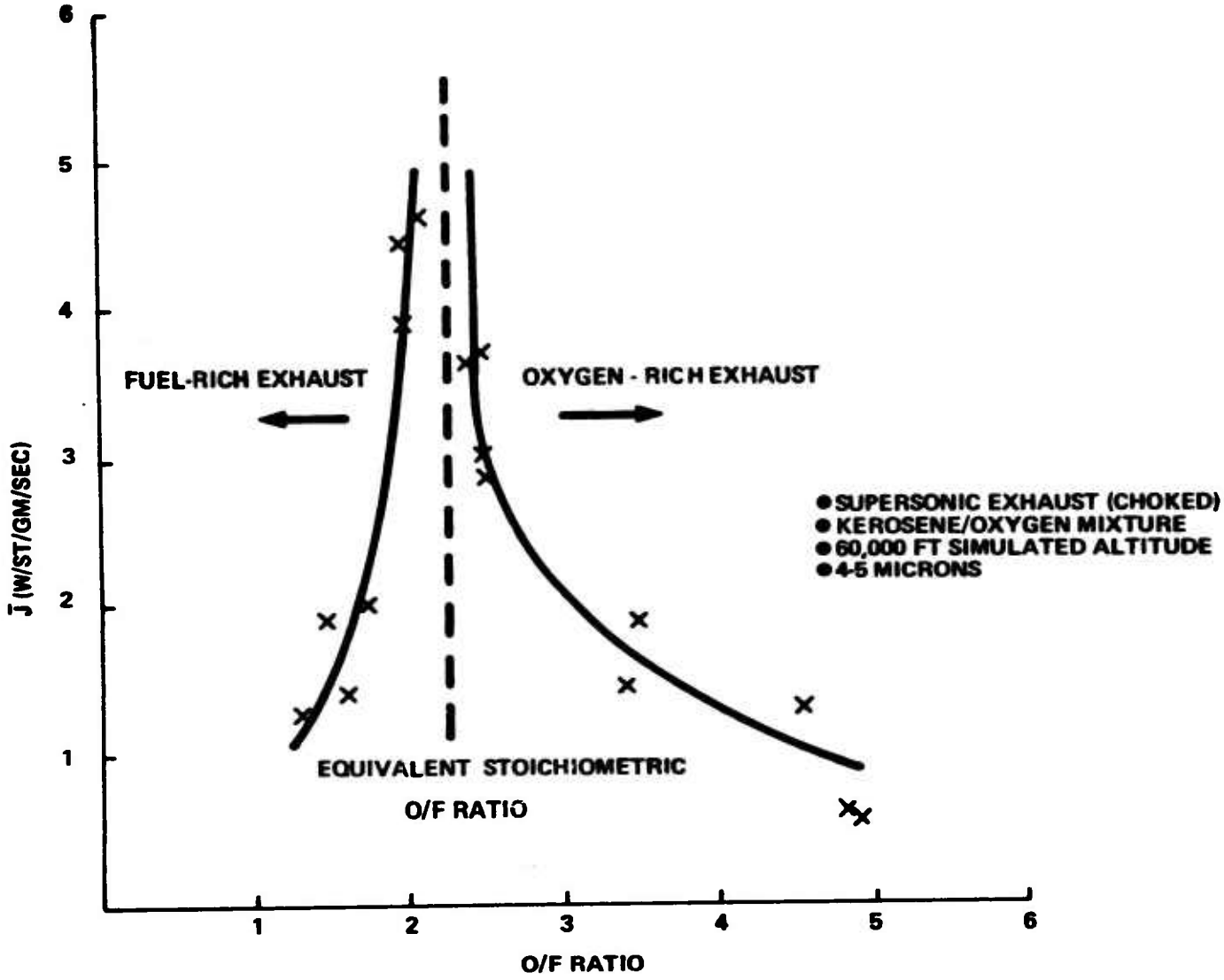

Figure 7. Final Relationship between $\bar{J}$ and O/F Ratio

KEROSENE/OXYGEN MIXTURE
60,000 FT ALTITUDE

OXYGEN-RICH, O/F > 3.5

OXYGEN-RICH, O/F > 2.5

OPTIMUM, O/F ~ 2.0

FUEL-RICH, O/F < 1.7

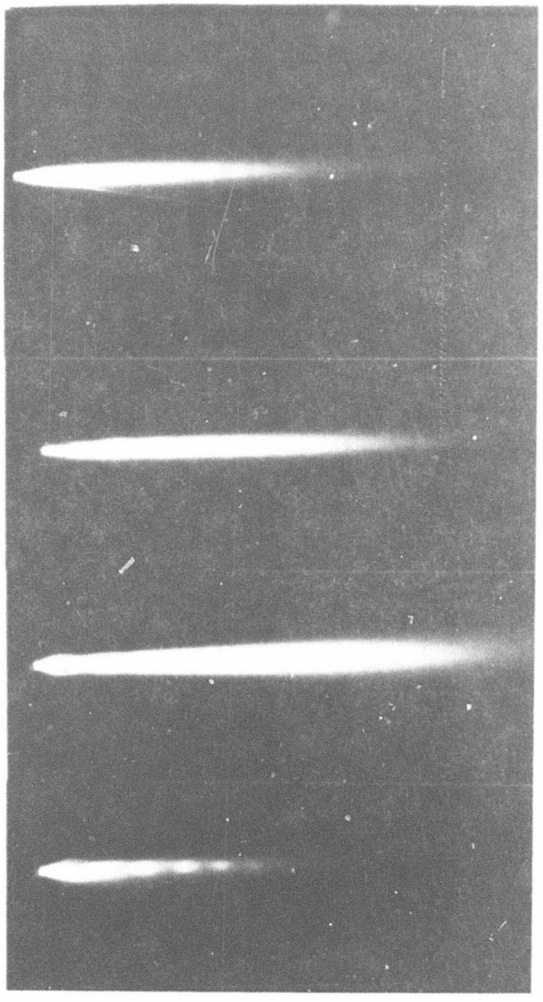

Figure 8. Effect of O/F Ratio on Plume Geometry.

At sea level static conditions the optimum occurs at an engine O/F ratio around 1.0 (Reference 1). As the altitude is increased to 60,000 feet, and the oxygen in the air ambient is decreased, additional oxygen is required from the engine to produce optimum combustion in the plume. The optimum O/F ratio thus shifts to a higher value (Reference 1 and Figures 6 and 7). The condition that is created in both cases is most probably stoichiometric for an extended combustion region which includes both the combustion chamber and the plume.

It can be concluded from these data that afterburning is a major mechanism in the creation of radiant energy for the altitudes of interest. The combustion process in the engine provides only part of the oxidizer required. Maximum radiation is <u>not</u> produced if the engine is operated with a stoichiometric mixture -- it is only produced when a fuel-rich mixture exits the engine nozzle and combusts with the oxygen in the air ambient. These conclusions thus lead to the modification of Figure 6 in the manner shown in Figure 7.

SECTION IV

CHOKING EFFECT

The infrared radiant intensity of an exhaust plume will change drastically depending on whether or not choked flow exists. For a fixed nozzle expansion ratio (Reference 4),

$$P_c/P_e = [1 + \frac{\gamma - 1}{2} M_e^2]^{\gamma/(\gamma - 1)} \quad (1)$$

where P_c = chamber pressure

P_e = ambient exit pressure

γ = specific heat ratio (assumed constant)

M_e = Mach number

Choked flow exists as long as $M_e > 1$ with the flow becoming unchoked, i.e., subsonic, when $M_e < 1$. Even though γ varies with temperature and pressure, an average value of 1.26 can be used without significant error. Thus when $M_e = 1$, the above reduces to

$$P_c = 1.808\ P_e$$

When the engine chamber pressure falls below this critical fraction of the ambient pressure the exhaust plume changes quite drastically. Figure 9 contrasts the plume of the unchoked kerosene/oxygen engine directly against that obtained under choked conditions. The data were obtained with the engine fitted with a sonic nozzle. The unchoked condition was created by increasing the pressure inside the altitude chamber while the engine operating conditions remained the same.

The engine which was thus operating choked, i.e., with a high enough chamber pressure, at 60,000 feet became unchoked as the altitude dropped below 10,000 feet. The change in the plume shape, and thus radiant intensity, was abrupt rather than gradual. In many cases, the engine turned itself off near the critical altitude and upon re-ignition was observed to have changed from one mode of operation to the other. Figure 9 also shows the variation in the critical chamber pressure as a function of altitude.

Similar data have been obtained at sea level with a much larger solid propellant ramjet burning a totally different mixture. Figure 10 shows the identical behavior of a United Technology Corporation (Sunnyvale, California) sonic nozzle ramjet with a plexiglas fuel. The difference in the color of the plumes is due to the difference in the O/F ratio in each engine. In the ramjet case, net internal diameters ranging from 1.5 to 4

References:

4. Hill, P.G. and Peterson, C.K.: Mechanics and Thermodynamics of Propulsion. P.47, Addison-Wesley, Reading, Mass., 1965.

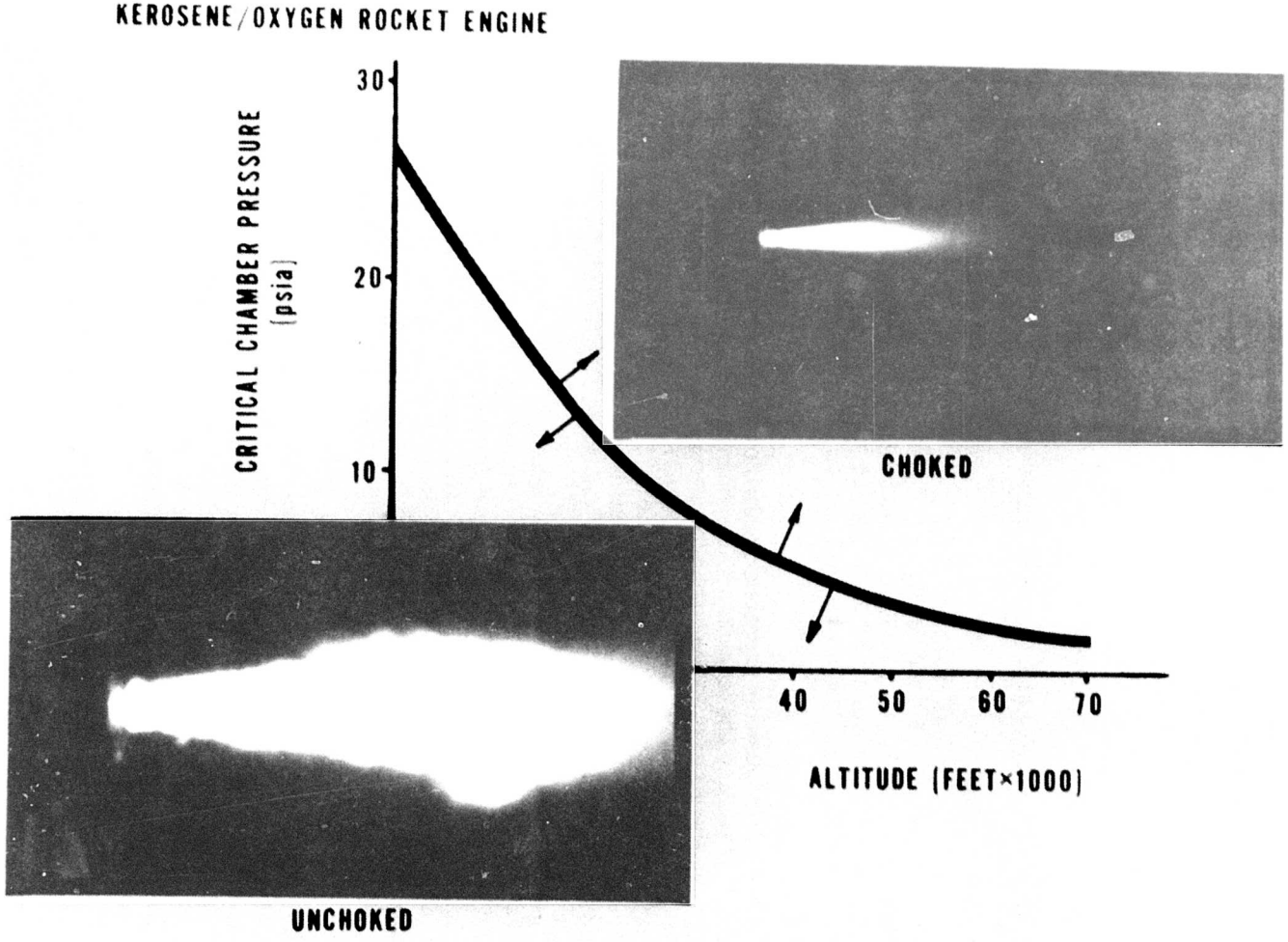

Figure 9. Effect of Choking on Rocket Engine Plume Volume.

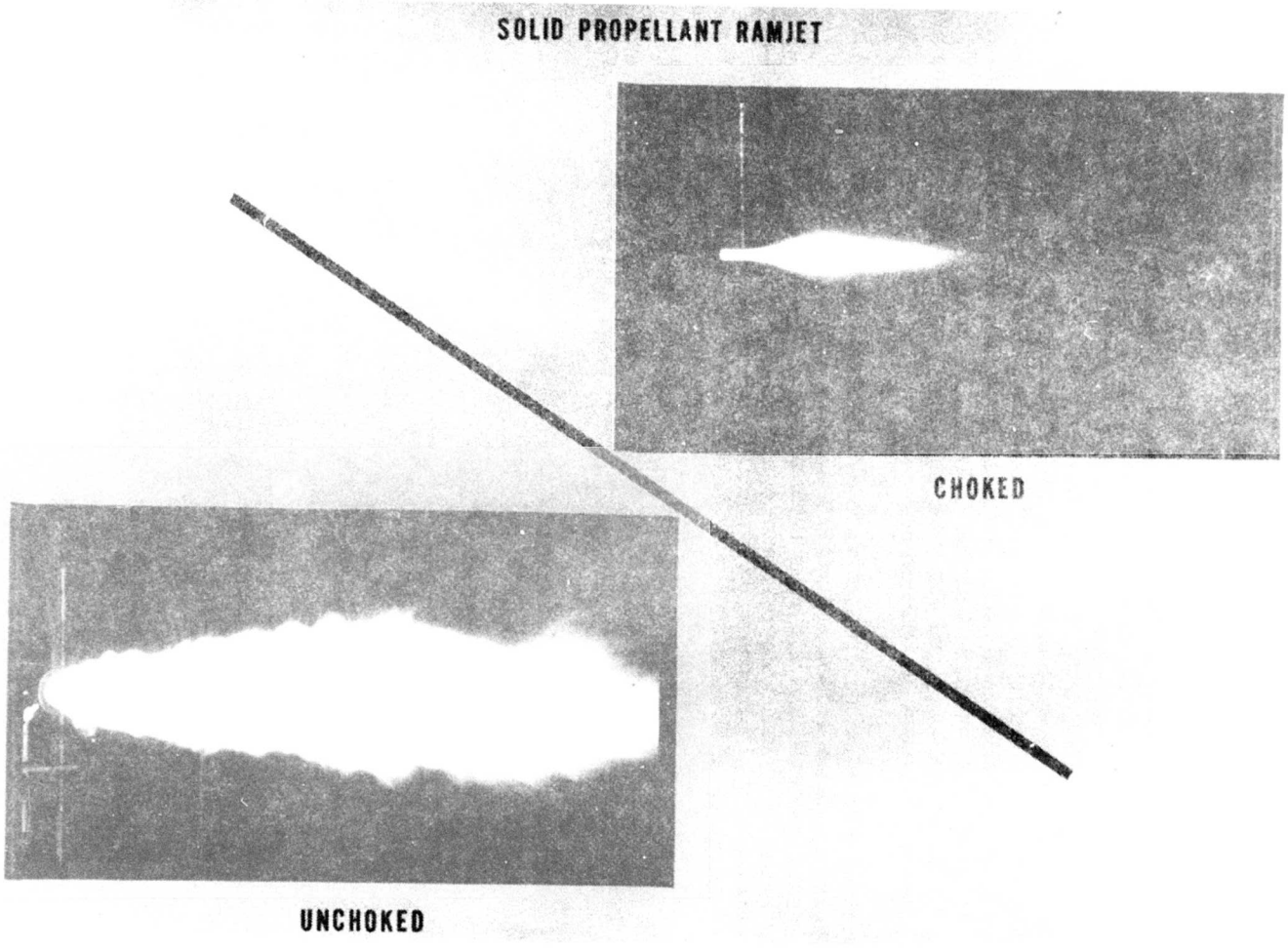

Figure 10. Effect of Choking on Solid Propellant Ramjet Plume Volume.

inches and mass flows from 50 to 200 grams/second were used. For both the rocket and the ramjet engine, the unchoked plume is a large flame with ragged edges. The choked plume is laminar, shorter and thinner. Operating in an unchoked combustion mode basically results in the engine chamber acting as a flameholder with most of the combustion occurring outside the engine chamber.

Under these static ambient conditions, and for both engines, the unchoked plume has a significantly higher figure of merit than the choked plume. Depending on O/F ratio and altitude, unchoked plumes have been observed to yield infrared figures of merit well over 300. On the other hand, the highest $\bar{J}$ observed to date for a choked plume is 7. Table 1 summarizes the figure of merit of a number of sources and shows the effect of choking on the figure of merit for all the infrared sources that have been considered for subscale targets. These data were obtained with the same experimental geometry and the same infrared instrumentation and are an update of the data presented in Reference 2.

An unchoked plume can be created with a simple mixing nozzle. The last two entries in Table 1 show the results obtained with such a nozzle using both kerosene/oxygen and a pyrophorics mixture atomized by nitrogen. It should be noted that while the pyrophoric/air mixture combusts at much higher temperatures than the kerosene/oxygen mixture, their maximum figures of merit differ very little.

TABLE 1. MAXIMUM FIGURES OF MERIT
(STATIC CONDITIONS)

	SEA LEVEL	60,000 FT
	(WATTS/STERADIAN/GRAM/SECOND)	
POPS ROCKET (NH_4ClO_4/Zr/C)		0.4
ROCKET (KEROSENE/OXYGEN)	1.0	7.0
RAMJET (JP4)	1.6	
HAST HYBRID ROCKET (POLYMER/IRFNA)	4.8	
SLURRY FLAMEHOLDER($NaNO_3$/HEPTANE/Mg)	20*	20*
RAM ROCKET (PLEXIGLAS)	97	
INJECTOR NOZZLE (KEROSENE/OXYGEN)	250	250
MIXING NOZZLE (PYROPHORICS)	300	300

*All the data in Table 1 were recorded with a single radiometer filter (Hewlett Packard Model 8330A) and are thus all consistent with each other. The slurry figure of merit was obtained with the last slurry flameholder and disagrees with the figure of merit of 90 reported earlier (Reference 5). The latter figure was measured with a different radiometer and with the slurry burning in an earlier flameholder. The lower figure of merit for the slurry reported in Table 1 could be due to disagreement between radiometers. However, it is more likely due to differences in chamber pressure (and thus degree of choking) between the earlier and the last flameholder. Numerous changes in the exhaust nozzle geometry of the slurry flameholder have occurred. If the degree of choking provided by the various exhaust nozzles were different, the infrared figure of merit would change significantly. The investigations on the effect of choking on the infrared figure of merit had not been made at the time the slurry flameholders were being designed and its impact could thus not have been taken into account.

References:

5. Ehrenzeller, D.G.: HAST/Slurry Prototypes. AFATL-TR-73-172, Eglin AFB, Florida, August 1973.

SECTION V

EXIT GAS VELOCITY AND THRUST EFFECT

The effect of exit gas velocity and thrust on the infrared plume radiation has been reported in detail (Reference 6). These measurements could only be made by holding constant key parameters such as the O/F ratio. Figure 11 summarizes the relationship between $\bar{J}$, exit gas velocity, and chamber pressure for the subscale kerosene/oxygen rocket motor. It was determined that, provided choked flow conditions exist, $\bar{J}$ for the 4 to 5 micron band does not vary to any significant extent with the exit gas velocity or the thrust.

References:

6. Drs. D.B. Ebeoglu, and K.E. Harwell: The Effect of Exit Velocity on the Infrared Radiation Intensity of an Exhaust Plume. AFATL-TR-74-10, Eglin AFB, Florida, January 1974.

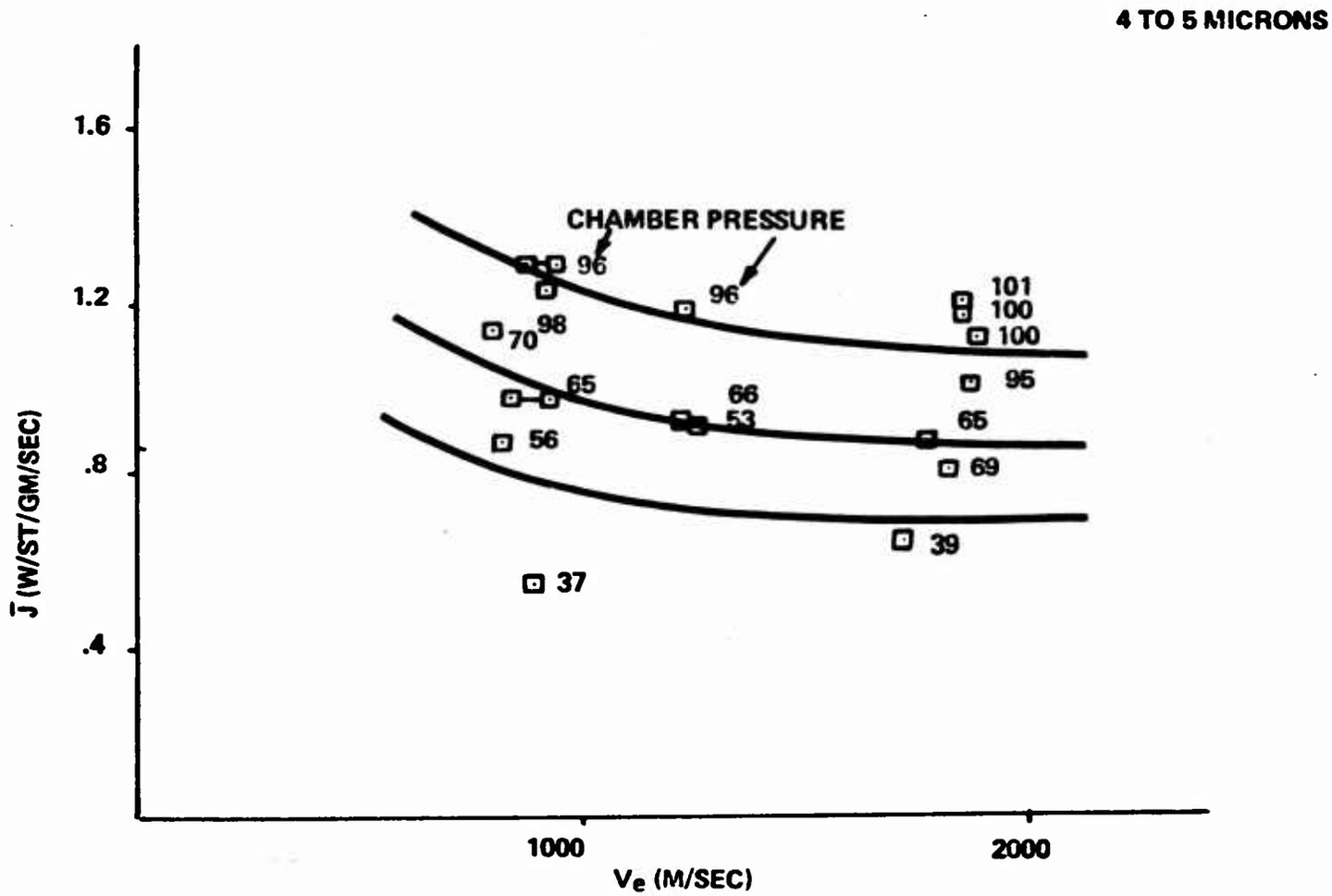

Figure 11. Effect of Exit Gas Velocity on $\bar{J}$.

SECTION VI

INFRARED RADIANT INTENSITY

Having discussed the various effects of operating parameters on the infrared figure of merit it is appropriate to cap the analysis by re-examining the direct relationship between infrared radiant intensity, J, to these parameters and to total mass flow rate, $\dot{m}$.

MASS FLOW RATE

The relationship between J and $\dot{m}$ for the 4 to 5 micron band is illustraded in Figure 12 for the case of an O/F ratio held constant at 3.5. The data were obtained using several sonic and supersonic nozzles. A linear relationship can be projected, although there is a fair amount of scatter in the data. The same linear variation of J with $\dot{m}$ is evident within the accuracy of all the data taken to date using varying mass flow rates with similar mixture ratios. The figure of merit can thus be used as a scaling factor to determine radiant intensity, given operating conditions and the value of the total mass flow rate.

The relationship between radiant intensity and other gas dynamics parameters can then be obtained from their relationship to the mass flow rate. The chamber pressure, P_c, can be shown to be directly proportional to $\dot{m}$ from the equation for characteristic velocity, C_* (Reference 4, p. 357),

$$C_* = \frac{P_c A_*}{\dot{m}} \tag{2}$$

where A_* = throat area for sonic and supersonic nozzles.

Figure 13 shows the linear variation between $\dot{m}$ and P_c measured with the kerosene/oxygen rocket motor. From these considerations, it follows that the infrared radiant intensity, J, is also directly proportional to chamber pressure.

THRUST

The relationship between thrust and infrared radiant intensity can be obtained in a similar fashion. From the equation for thrust, T, (Reference 4, p. 356),

$$T = \dot{m}\ u_e + (P_e - P_a)\ A_e \tag{3}$$

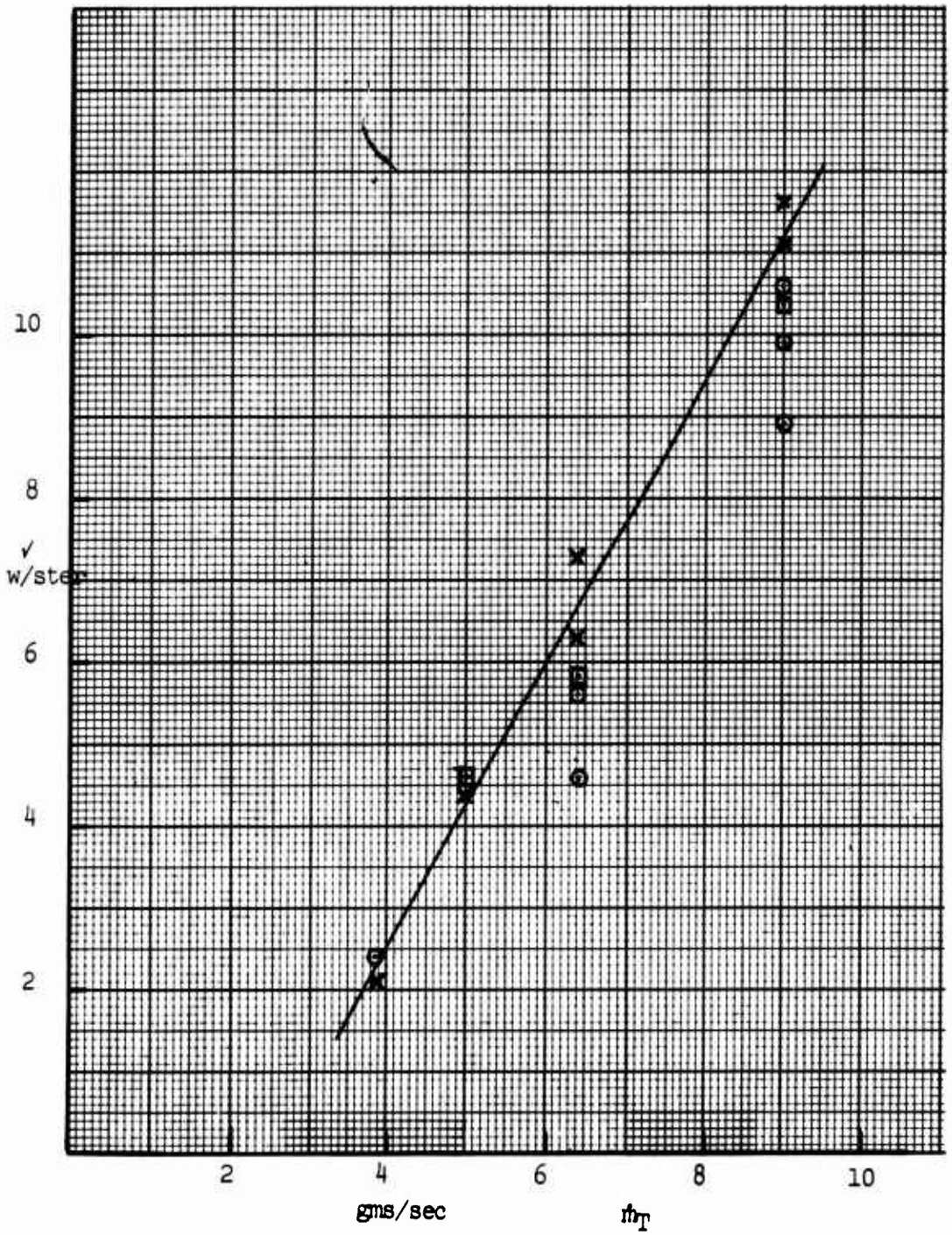

Figure 12. Radiant Intensity as a Function of Mass Flow

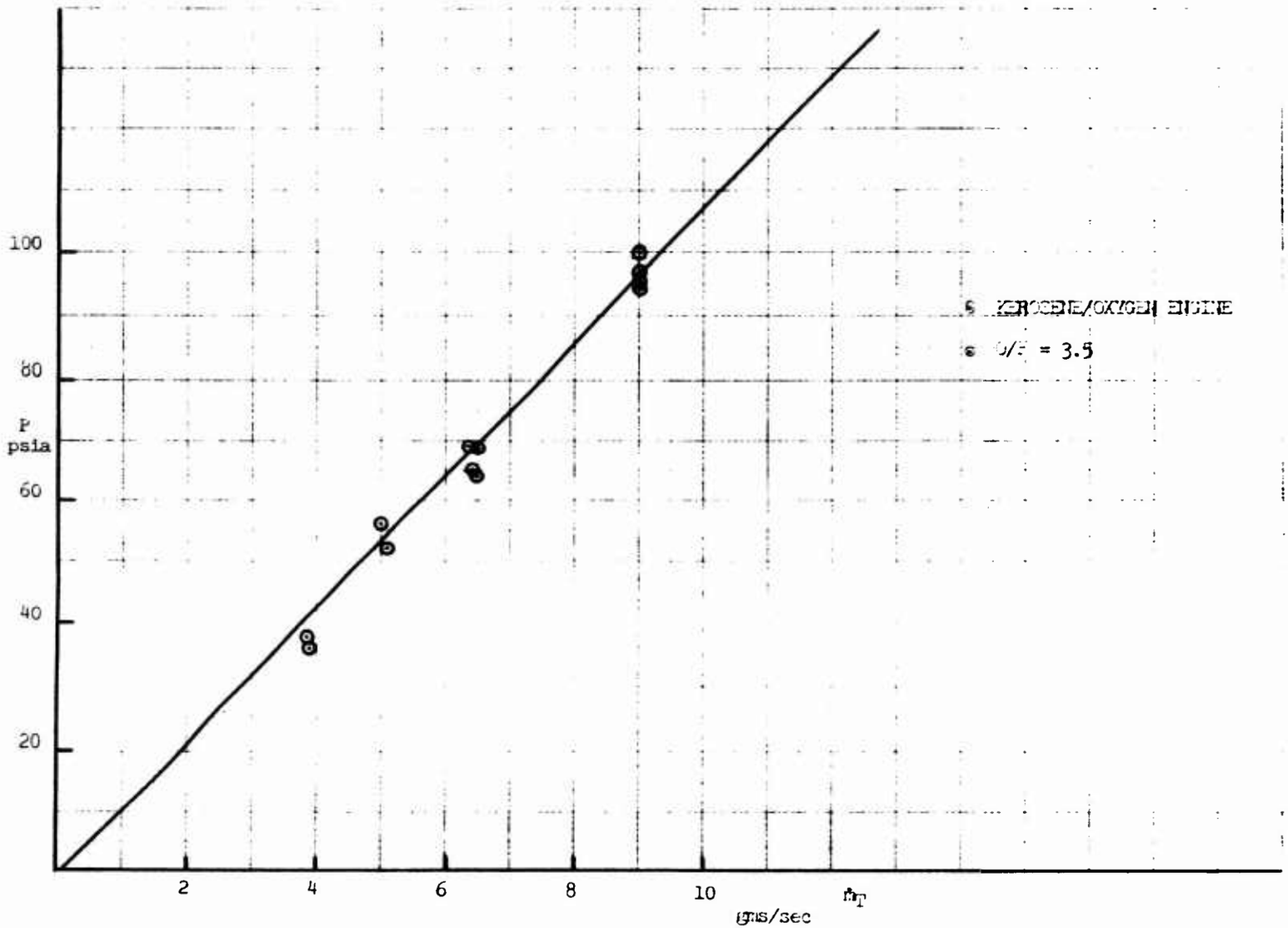

Figure 13. Pressure Versus Total Mass Flow Rate for Kerosene/Oxygen Engine

where u_e = exhaust gas velocity

P_e = exhaust pressure

P_a = ambient pressure

A_e = exit area

which can be shown for the test engine to reduce to

$$T = \dot{m}\ u_e + (P_c/12 - P_a)\ A_e \text{ for } A_e/A_* = 2.4; \tag{4}$$

assuming $\dot{m} = k_o P_c$ from Equation (3), Equation (4) results in

$$T = \dot{m}\ (u_e + k_1) - k_2, \text{ where } k_1 = 1/12k_o \text{ and } k_2 = P_a A_e \tag{5}$$

Figure 14 shows the experimental verification of the linear relationship between thrust and mass flow rate predicted by Equation (5). The data were obtained for one of the sonic and one of the supersonic exit nozzles of the kerosene/oxygen rocket engine. It can thus be concluded that radiant intensity will be directly proportional to thrust, since thrust is directly proportional to mass flow, while the figure of merit will not vary with thrust.

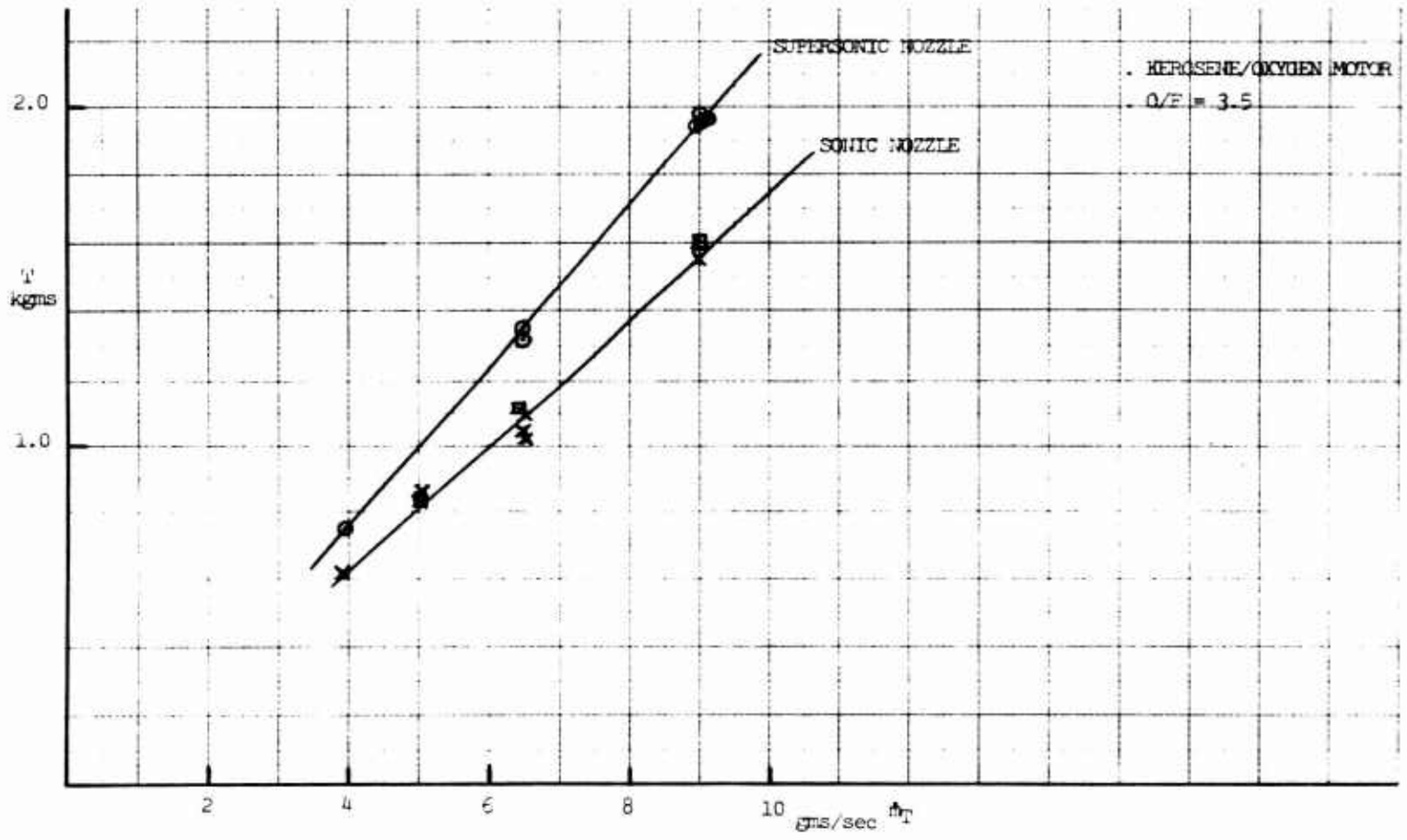

Figure 14. Thrust Versus Total Mass Flow Rate for Kerosene/Oxygen Engine

SECTION VII

CONCLUSIONS AND RECOMMENDATIONS

The objective of the report has been to show how key gas dynamics parameters affect the infrared radiant intensity of propulsion devices. Although there are many methods of propulsion, the underlying principles are few. Therefore, the conclusions reached using a rocket engine are applicable to other engines. An attempt has been made to close the gap between the variable parameters available to the designer of the engine and the behavior of the infrared signature. A specific problem, that of threat simulation by subscale targets within specific flight envelopes, has been addressed. Fundamental parameters have been shown, under these conditions, to have practical and significant effects.

Theoretical studies should now be carried out to verify models, obtain deeper understanding of the principles themselves, and provide valid predictive tools. This interaction will permit cost effective analytic extrapolations to be performed. It will also permit a fuller range of engineering implications to be clearly seen prior to advancing to prototype systems.

It should be stressed that the fundamental study of the turbojet engine radiation simulation, which involves so many disciplines, cannot be completed without a significant effort made to perform a similar parametric analysis in chemistry. Such an investigation is not only desirable, but also essential since any solution to the problem is clearly payload limited.

Microscopic behavior should continue to be the primary aim of the investigation. Some microscopic processes, namely the interaction of discrete particles such as carbon with a plume, are of interest and basic research in these specific cases is recommended. Finally, the last major boundary condition, that of a co-flowing airstream, should be examined in great detail before the fundamental performance investigations are concluded.

(The reverse of this page is blank)

INITIAL DISTRIBUTION

USAF (RDPA)	1	ASD (XRHP)	1
USAF (RDQRM)	1	AFAPL (SD)	1
USAF (XOOWQB)	1	AFOSR (NAE)	1
AFSC (DLC)	1	USA MC (AMSMI REI)	1
AFSC (DLXP)	1	USNWC (Code 4513)	1
AFSC (INH)	1	USNWC (Code 454/45403)	1
AFSC (SDAS)	1	USNWC (Code 4543)	1
AFSC (SDRA)	1	IDA (Dr Hans Wolfhard)	1
AFSC (SDWA)	1	USA MC (AMSMI-TM)	1
TAC (DRF)	1	Ogden ALC (MMNOP)	1
AFAL (NV)	1	TRADOC (TAWC-DO)	1
ASD (ENYS)	1	TAWC (TEF)	1
ASD (RWDD)	2	TAWC (TEFA)	1
FTD (PDJR)	5	ADTC (TGWN)	1
WRAMA (MMY)	1	ADTC (TSGPA)	1
ADC (XPAW)	1	AFATL (DL)	1
RADC (IRAP)	1	AFATL (DLB)	1
6585 Test Gp (TD)	1	AFATL (DLOSL)	2
AFWL (DOGL)	1	AFATL (DLMM)	1
AU (AUL/LSE-70-239)	1	AFATL (DLMQ)	12
Sandia Corp Tech Lib 3421	1		
ADWC 4750 Test Sq	4		
USNRL (Code 7780)	1		
ODDR&E OSD/Combat Support	1		
ARPA (TIO)	1		
NASC (AIR 5352)	2		
NASC (Aero Tgts Proj APC 247)	1		
II&AC Univ of Mich	1		
SAMSO (SYJ)	1		
NMC (Code 5160)	1		
DASA Info & Anal Ctr GE TEMPO	1		
The RAND Corp (Lib D)	1		
USNWC (Code 3051)	1		
USNWC (Code 4514)	1		
USN ADC (AME-1)	2		
USN ADC (AME-2)	2		
Redstone Sci Info Ctr (Doc Sec)	2		
Battelle Memorial Inst (Rpts Lib)	1		
IDA Class Lib	1		
WSMR (STEWS-ID-IE)	1		
AEDC (ARO, Inc) Doc Lib	1		
DDC	2		
USAF (SAMI)	1		
AFSC (DLCAW)	2		
AFRPL (DYSP)	1		
AFCRL (LKC)	1		
AFAPL (RJT)	1		

(The reverse of this page is blank)